Physics Letters A 381 (2017) 2860–2865

Contents lists available at ScienceDirect

Physics Letters A

www.elsevier.com/locate/pla

Designing quantum resonant scatterers at subwavelength scale

Jeng Yi Lee [a], Andrey E. Miroshnichenko [b], Ray-Kuang Lee [a,c,*]

[a] Institute of Photonics Technologies, National Tsing Hua University, Hsinchu 300, Taiwan
[b] Nonlinear Physics Centre, Research School of Physics and Engineering, The Australian National University, Canberra 2601, Australia
[c] Physics Division, National Center for Theoretical Sciences, Hsinchu 300, Taiwan

ARTICLE INFO

Article history:
Received 27 May 2017
Accepted 28 June 2017
Available online 3 July 2017
Communicated by A. Eisfeld

Keywords:
Quantum transport
Scattering theory
Quantum dots
S-matrix method in transport

ABSTRACT

For an isotropic quantum resonant scatterer, such as a quantum dot embedded in host semiconductors, we propose a method to achieve resonant electron scattering by taking physical quantities into account through the second-order expansion. All needed physical information for spherical harmonic channels in anomalous quantum resonant scattering is revealed in a parameter space as the size of quantum scatterer is comparable to the de Broglie wavelength of incoming matter wave. Our results provide the guideline to realize quantum resonant scatterers with state-of-the-art semiconductor heterostructure technology.

1. Introduction

Wave phenomena from different origins share the same principle of superposition, which can be controlled by properly designed structures. In optics, the study on light scattering by subwavelength particles can be traced back to Lord Rayleigh in early developments to explain the colors in the sky [1]. Based on Lorenz–Mie theory, anomalous light scattering in small particles due to the localized surface plasmonic mode is found when the permittivity, ϵ, of a lossless particle at subwavelength scale meets the resonant condition, i.e., $\epsilon = -\epsilon_m\,(l+1)/l$. Here, ϵ_m corresponds to the permittivity of the surrounding environment, and l denotes the index for spherical harmonics channels ranging from $l = 1, 2, \ldots \infty$ [2,3]. Nowadays, with state-of-the-art nano-structured technologies, having an efficient way to manipulate and design nano-optics is desirable. Due to such a great enhancement in the near-field, lots of potential applications have been demonstrated on light harvesting, sensing, medical treatment and so on [4–10].

Based on the analogies between classical electrodynamics and quantum mechanics, applying concepts from electromagnetic metamaterials to other areas of physics has received considerable attention [11–15]. For barrier-well potentials formed in a core-shell nano-particle embedded in a host semiconductor material, the cloaking as well as invisibility for the electronic transport are revealed by the scattering cancellation method [16–18]. Quantum cloaking can enhance carrier mobility [19] and may be realized in various solid state systems, such as quantum dots and graphenes [20,21].

Even though similar approaches can be applied both to classical electromagnetic and quantum matter waves, the underlying physical interpretations are different. Through the similar mathematical structure between the Helmholtz wave equation and time-independent Schrödinger equation, there exists the correspondence between the permittivity for electric fields in dielectric materials to the effective mass for quantum wavefunction in potentials. Nevertheless, unlike the classical electrodynamics, the index for spherical harmonics channels in quantum waves starts from $l = 0$, which corresponds to the s-wave scattering. Then, the effective mass information (m^*) for a quantum scatterer is totally missing when $l = 0$, if we only apply the first order expansion to meet the resonant condition.

To solve this problem, we can not rely on the conventional Born approximation that only deals with weak scattering interaction [22]. Physically, the results obtained by first approximation indicate that a quantum particle would be intrinsically deflected with a small angled to the original momentum direction. However, in this work, to meet the quantum resonant scattering, a maximized scattering is expected to accompany with a large momentum transfer. To go beyond the Born approximation, we expand the corresponding spherical Bessel and Neumann functions up to the second-order terms, only with which we can include effective mass and potential into the possible implementation for quantum resonant scatterers. By parameterizing system variables, we show

* Corresponding author.
E-mail address: rklee@ee.nthu.edu.tw (R.-K. Lee).

http://dx.doi.org/10.1016/j.physleta.2017.06.051
0375-9601/

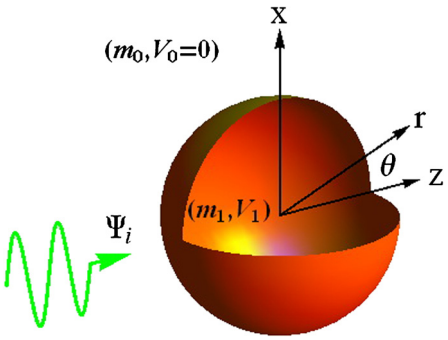

Fig. 1. (Color online.) A schematic view of matter wave scattering by a spherical quantum resonant scatterer. The isotropic and homogeneous effective mass and potential energy inside the scatterer and in the environment are denoted as (m_1, V_1) and $(m_0, V_0 = 0)$, respectively. An incident plane wave for the transport electron, Ψ_i, is assumed to propagate along the z-axis.

a contour plot including all system parameters to satisfy the resonant condition for various quantum angular momentum channels ($l = 0, 1, 2, ..$). A remarkable agreement is also shown in the comparison of our analytical results to the full numerical calculations.

This work seeks for opposite extreme limit in elastic scattering process, quantum resonance scattering, since it can make quantum particles scattered to large directions, equivalent to large momentum transfer occurred with some non-negligible probability. Such anomalous quantum scatterers are desirable for a variety of applications, such as the enhancement of thermoelectric power factor by embedding resonant carriers in thermoelectric materials [23–25], the scanning probes for bosonic atom collisions at ultracold temperatures [26,27], and the observation of quantum proximity resonances [28]. A realistic case has been proposed in semiconductor quantum dots, such as GaAs/$Ga_{1-x}Al_xAs$ materials [29]. In general, in the vicinity of a resonance with respect to energy it is not always possible to employ a characteristic Breit–Wigner formula for the scattering cross section [30], as the profile becomes an symmetric one [31].

By applying our result to a quantum scatterer in the shape of a finite-size sphere, such as a quantum dot, with an isotropic and homogeneous effective mass and potential for the electron transport in a host semiconductor, we also propose a set of alloy semiconductor materials to achieve the s-wave resonance. Our approach provides a compact solution to the practical question on how to build a resonant quantum scatterer precisely for various angular momentum channels when the real material properties are taken into consideration.

2. Theory

We start our analysis by studying the scattering properties of a finite-size spherical scatterer of the radius a, which can be considered as a quantum dot, a dopant or a nanoparticle, see Fig. 1. Such quantum scatterer has isotropic and homogeneous effective mass and local potential, denoted as m_1 and V_1, respectively. The environment could be a host semiconductor with its effective mass m_0 and potential V_0. Without loss of generality, the potential in the surrounding environment can be set to zero, i.e., $V_0 = 0$. The incident quantum matter wave of a single transport electron is assumed to be a plane wave propagating along the z direction, which can be described by the effective Schrödinger equation in time-independent form:

$$-\frac{\hbar^2}{2}\vec{\nabla}\cdot[\frac{1}{m^*(\vec{r})}\vec{\nabla}\psi] + [V(\vec{r}) - E]\psi = 0. \tag{1}$$

Here, the spatial wave function ψ, the effective mass m^*, the effective potential V, and the total energy E are denoted for a single electron, respectively. In the following, we also restrict our study to a Hermitian quantum system with real potentials only. In this scenario, the total probability for the wave function of our transport electron is conserved due to only elastic scattering processes involved. To have a real value in the propagation wavenumber, $k_0 = \sqrt{2m_0E}/\hbar$, both the incident energy E and the effective mass in the environment m_0 are taken to be positive.

As we are dealing with a central scattering potential having rotational invariance, the Hamiltonian commutes with L^2 and L_z, where L is the quantum angular momentum operator. Thus, we can use the eigenstate of L^2 to express the wave function in our scattering system. By using these eigenstates, we express the environmental wave function, ψ_{env}, including incident plane wave and scattering wave: $\psi_{env}(r,\theta) = e^{ikr\cos\theta} + \psi_{scat} = \sum_{l=0}^{l=\infty} i^l(2l+1)[j_l(k_0a) + a_l^{scat}h^{(1)}(k_0a)]P_l(\cos\theta)$. Here, l denotes the quantum angular momentum for the corresponding channel, j_l is spherical Bessel function, a_l^{scat} represents scattering coefficient determined by the radiating boundary conditions, $h^{(1)}$ is the first-kind of spherical Hankel function due to its out-going property for scattering matter wave, and $P_l(\cos\theta)$ is the Legendre polynomial. Meanwhile, inside the scatterer, there exists a transmitted wave written as $\psi_{tr}(r,\theta) = \sum_{l=0}^{l=\infty} i^l(2l+1)t_l j_l(k_1r)P_l(\cos\theta)$, where t_l is unknown transmitted coefficient also determined by boundary conditions and k_1 is transmitted wavenumber defined as $\sqrt{2m_1(E-V_1)}/\hbar$. As our quantum scatterer has the azimuthal symmetry with respect to the rotation around the propagation z-axis, the scattering and transmitted matter waves are also ϕ independent, as expected.

With the continuity of wave function at the boundary and the conservation of probability flux along the radial direction, i.e., $\psi_{env}(a,\theta) = \psi_{tr}(a,\theta)$ and $(1/m_0)(\partial\psi_{env}/\partial r)|_{r=a} = (1/m_1)(\partial\psi_{tr}/\partial r)|_{r=a}$, respectively, one can calculate the two unknown complex coefficients: a_l^{scat} and t_l. Moreover, the scattering coefficient a_l^{scat} can be written in a compact form,

$$a_l^{scat} = -\frac{\zeta_l}{\zeta_l + i\eta_l}, \tag{2}$$

where ζ_l and η_l are:

$$\zeta_l = \frac{k_1}{m_1}j_l'(k_1a)j_l(k_0a) - \frac{k_0}{m_0}j_l'(k_0a)j_l(k_1a) \tag{3}$$

and

$$\eta_l = \frac{k_1}{m_1}j_l'(k_1a)y_l(k_0a) - \frac{k_0}{m_0}y_l'(k_0a)j_l(k_1a), \tag{4}$$

with the spherical Neumann function denoted by $y_l(x)$. Furthermore, to quantify the scattering efficiency, an integration over a closed area can be performed by calculating the scattering probability flux $\vec{J}_{scat}$ at the far field zone (that is $r \to \infty$) per unit incident matter current, $|\vec{J}_{in}| = \hbar k_0/m_0$. With this concept, we can define the scattering cross section accordingly [2]:

$$\sigma^{scat} = \frac{\oint \vec{J}_{scat}\cdot\hat{r}da}{|\vec{J}_{in}|} = \frac{4\pi}{k_0^2}\sum_{l=0}^{l=\infty}(2l+1)|a_l^{scat}|^2, \tag{5}$$

and the transport cross section has the following form:

$$\sigma^{tr} = \oint(1-\cos\theta)\frac{d\sigma^{scat}}{d\Omega}d\Omega \tag{6}$$

$$= \frac{4\pi}{k_0^2}\sum_{l=0}^{l=\infty}(2l+1)|a_l^{scat}|^2 - \frac{8\pi}{k_0^2}\sum_{l=0}^{l=\infty}(l+1)Re[(a_l^{scat})^*a_{l+1}^{scat}], \tag{7}$$

which also provides a quantity to measure the level of probabilistic direction of momentum change with respect to incident momentum.

As a rule of thumb, the major contributing terms for these convergent series depend on the environmental size parameter, $k_0 a$ [2,17,18,22]. As a result, at the subwavelength scale, i.e., $k_0 a < 1$, the monopole ($l = 0$, or called as the s-wave channel) and the dipole ($l = 1$, or called as the p-wave channel) play important roles in the scattered matter wave. We should remark that there is another equivalent expression for scattering coefficient via a phase shift, δ_l, by setting $e^{i2\delta_l} = 1 + 2a_l^{scat}$, which is related to S-matrix element [22]. However, the representation a_l^{scat} for scattering cross section is more flexible to seek for specific scattering solutions.

Note that, the above derivations and formulas share the analogy to those in the electromagnetic Mie theory. From Eq. (2), the conditions to have scattering resonance and invisible conditions for each channel are achieved for $\eta_l = 0$ and $\zeta_l = 0$, respectively, leading to $4\pi(2l+1)/k_0^2$ and 0 in the scattering cross sections for the l-th angular momentum channel. Moreover, it has been pointed out that electromagnetic resonant scattering comes from the localized surface plasmon condition, $\epsilon = -\epsilon_m(l+1)/l$ for lossless subwavelength particles [2,3]. However, such a condition for localized surface plasmon is only satisfied for the electrical extremely small limit, which is independent of size in scatterers. In the following, we give a systematic way to design quantum scatterers to have the resonance condition beyond this electrical small approximation, by taking second-order terms in the expansions into consideration. In this way, the characteristic equation to satisfy the resonance at lth channel would involve all physical parameters in our system.

3. Results and discussion

For a given quantum scatterer, there are five independent system parameters, i.e., (a, E, m_0, m_1, V_1), corresponding to the geometric radius of a spherical scatterer, the incident energy, the effective mass in the environment, the effective mass inside the scatterer, and the potential inside the scatterer, respectively. To obtain the resonant scattering condition for these five system parameters, we expand the corresponding spherical Bessel $j_l(x)$ and spherical Neumann function $y_l(x)$ up to the second-order terms, in order to go beyond the extremely small limit. So, up to the second-order terms, one has

$$j_l(x) \approx \frac{x^l}{(2l+1)!!}\left[1 - \frac{x^2}{2(2l+3)} + O(x^4)\right], \tag{8}$$

$$y_l(x) \approx -\frac{(2l-1)!!}{x^{l+1}}\left[1 + \frac{x^2}{2(2l-1)} + O(x^4)\right]. \tag{9}$$

Note that the inaccuracy between second-order approach and exact functions can be less than 5% even for $|x| \sim 1$. Then, with the second-order terms in Eqs. (8)–(9) the corresponding ζ_l and η_l shown in Eqs. (3)–(4) can be approximate as

$$\begin{aligned}\zeta_l \approx{}& \frac{(k_0a)^l(k_1a)^l}{4a(2l+3)^2[(2l+1)!!]^2}\{\frac{1}{m_1}[-2(2l+3)+(k_0a)^2] \\ &\times[-2l(2l+3)+(l+2)(k_1a)^2] \\ &-\frac{1}{m_0}[-2l(2l+3)+(l+2)(k_0a)^2][-2(2l+3)+(k_1a)^2]\},\end{aligned} \tag{10}$$

$$\begin{aligned}\eta_l \approx{}& \frac{(2l-1)!!k_0(k_0a)^{-(l+2)}(k_1a)^l}{4(2l-1)(3+2l)(2l+1)!!}\{\frac{1}{m_0}[-4l-6+(k_1a)^2] \\ &\times[4l^2+2l-2+(l-1)(k_0a)^2] \\ &+\frac{1}{m_1}[-2+4l+(k_0a)^2][-4l^2-6l+(l+2)(k_1a)^2]\}.\end{aligned} \tag{11}$$

When we substitute these second-order approximated results into the scattering coefficient a_l^{scat}, for $l = 0$ and $l \geq 1$, the corresponding leading orders become $(k_0a)^3$ and $(k_0a)^{2l+1}$, respectively. As a result, at subwavelength scale, main contribution to scattering cross section in normal case would be s- and p-wave channels. Moreover, it is expected that one should simultaneously eliminate these two channels to achieve invisibility [16–21].

Then, for the resonance condition to have a maximized scattering, the requirement of $\eta_l = 0$ for each angular momentum channel, l, we can be written in the following characteristic polynomial equation:

$$\begin{aligned}&\frac{m_1}{m_0}[-4l-6+(k_1a)^2][4l^2+2l-2+(l-1)(k_0a)^2] \\ &= -[-2+4l+(k_0a)^2][-4l^2-6l+(l+2)(k_1a)^2].\end{aligned} \tag{12}$$

In the subwavelength approximation, $k_0 a \ll 1$ and $|k_1 a| \ll 1$, Eq. (12) would be approximately reduced to the resonance condition, $m_1 = -m_0 l/(l+1)$. Moreover, we want to emphasize again that the system parameters, (a, k_0, k_1) or equivalently (a, E, V_1), will not be involved within the first-order expansion. These parameters, in particular, a, E and V_1 should be necessary for the implementation of semiconductor heterostructures when we take the system geometry, energy-band gap, and effective mass into consideration. Moreover, serious problems emerge in solid state systems, for the reason that the effective mass is a material dependent parameter, which is related to the dispersion relation of energy band structures for semiconductor materials with an effective potential V_1. Only with the second-order terms, as shown in Eq. (12), these system parameters can be all involved toward possible experimental realizations.

Even though we only have one characteristic polynomial equation, Eq. (12), to satisfy the resonant scattering condition, we parameterize the system variables to seek for resonance condition. Now, we define the ratio between two effective masses as m_1/m_0, the size parameter in the environment as $k_0^2a^2 = 2m_0Ea^2/\hbar^2$, and the corresponding size parameter in the scatterer as $k_1^2a^2 = 2m_1(E-V_1)a^2/\hbar^2$. Note that, the range for these two size parameters are bounded automatically due to the physical constraints and validity of approximation, i.e., $0 < k_0^2a^2 < 1$ and $-1 < k_1^2a^2 < 1$. Based on these three normalized variables, in Fig. 2, we show the parameter space, defined by m_1/m_0 and $k_0^2a^2$, for the solutions in the resonant scattering condition shown in Eq. (12). In Fig. 2, the colored contour lines in the plot indicate the corresponding value for the size parameter in the scatterer $k_1^2a^2$; while the background regions stand for undesirable solutions, for which the requirement $-1 < k_1^2a^2 < 1$ is not satisfied.

The resonant scattering condition for different channels can be all found in such a parameter space. In Fig. 2, we reveal the analytic solutions of Eq. (12) for s-wave ($l = 0$) in (a); for p-wave ($l = 1$) in (c); and for d-wave ($l = 2$) in (e), respectively. In addition to the analytical ones, we also apply numerical calculations directly to Eq. (4) with the requirement on $\eta_l = 0$, i.e., for s, p, and d-waves in Fig. 2 (b, d, f), respectively. With the comparisons between Fig. 2 (a, c, e) and (b, d, f), one can find a good agreement in our second-order approximation formula and exact numerical solutions.

We want to emphasize that one may apply numerical calculation directly to find resonant parameters, but only for a few variables by scanning the whole parameter spaces. In this scattering problem, we have five unknown parameters: (a, E, m_0, m_1, V_1), which becomes a challenge to solve even with a brute force approach. As seen from Fig. 2, one can also easily exclude the parameters in the uncolored regions, where the quantum resonance is not supported. Only through the contour plots shown in Fig. 2, we can successfully include all system parameters (a, E, m_0, m_1, V_1)

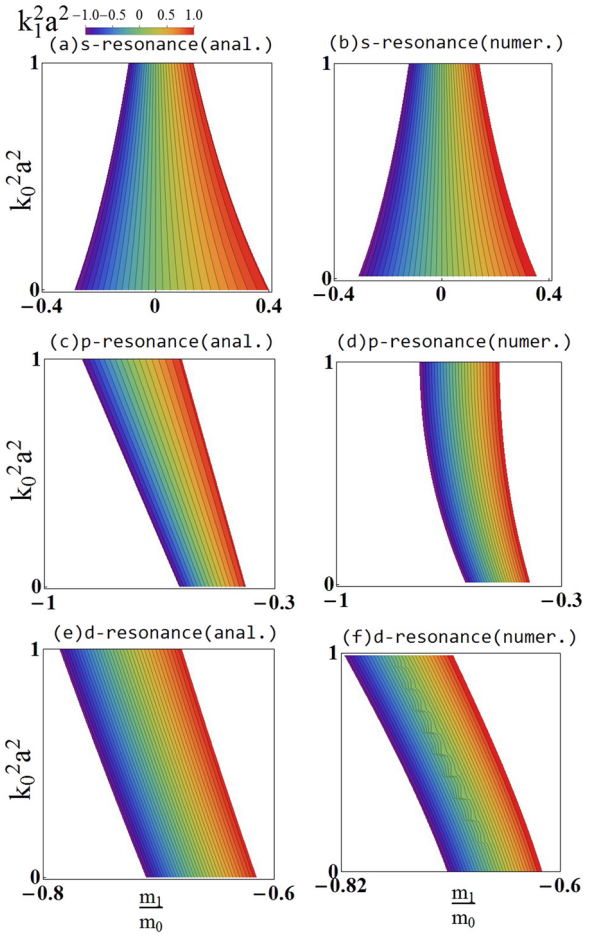

Fig. 2. (Color online.) The parameter spaces to satisfy the resonant scattering condition given in Eq. (12), illustrated in the contour plot defined by the ratio in the effective mass m_1/m_0 and the size parameter in the environment $k_0^2a^2$. The colored-contour lines indicate the corresponding value for the size parameter in the scatterer $k_1^2a^2$. The resonance conditions are shown for different channels: (a–b) s-wave ($l=0$), (c–d) p-wave ($l=1$), and (e–f) d-wave ($l=2$), respectively. The results in the left column (a, c, e) are generated by the analytical formula in Eq. (12); while the results in the right column (b, d, f) are solutions obtained directly from Eq. (4) with the requirement on $\eta_l=0$.

into one single map, which provides a compact and efficient way to design quantum resonant scatterers. To satisfy the resonance condition in each channel, from Fig. 2, we find that the sign in the ratio (m_1/m_0) plays an important role. To induce p-wave and d-wave resonant scattering conditions at the subwavelegnth scale, the corresponding effective mass in the quantum scatterer must be a negative one. On the contrary, for s-wave resonance, both positive and negative effective mass can meet this condition. As for the potential of the scatterer, we find that both potential barrier and potential well can satisfy the resonant condition, which differs from the examples illustrated in Ref. [29], where a well potential is needed in order to induce the resonance.

By applying the resonance condition, the corresponding resonant potential $V_{1,res}$ in each channel's resonance can also be found analytically within the introduction of second-order terms:

$$V_{1,res}(l,m_1,E,a,m_0) \tag{13}$$
$$= E - \frac{\hbar^2(2l+3)}{m_1a^2}\times\{\hbar^2(2l-1)[m_1(l+1)+m_0l]$$
$$+m_0a^2E[m_1(l-1)+m_0l]\}$$

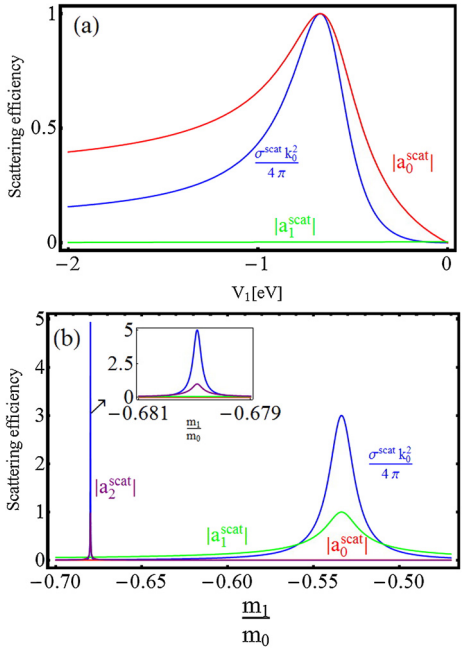

Fig. 3. (Color online.) Scattering and transport efficiencies, $\sigma^{scat}k_0^2/4\pi$ and $\sigma^{tr}k_0^2/4\pi$, are shown as a function of (a) the potential in the scatterer V_1, and (b) the ratio between two effective masses m_1/m_0. In addition, the decomposed magnitudes in scattering coefficient $|a_l^{scat}|$ for lowest-order channels are also depicted, for (a) $l=0,1$ and (b) $l=0,1,2$, respectively. Inset in (b) is the enlarged image to indicate the resonant scattering at d-wave ($l=2$). Here, the parameters used are (a): $a=1.3$ nm, $E=0.02$ eV, $m_0=0.1m_e$, and $m_1=0.03m_e$; (b): $m_0=0.2m_e$, $V_1=-0.01$ eV, $E=0.02$ eV, and $a=1$ nm.

$$\times\{\hbar^2(2l-1)[m_1(l+1)+m_0(l+2)]$$
$$+m_0a^2E[m_1(l-1)+m_0(l+2)]\}^{-1}.$$

Based on Eq. (13), in Fig. 3 (a), we report the scattering efficiency for s wave by tuning potential in the scatterer V_1. For the parameter set: $a=1.3$ nm, $E=0.02$ eV, $m_0=0.1m_e$, and $m_1=0.03m_e$, our analytical formula shown in Eq. (12) gives $V_1=-0.61$ eV; which is very close to the value $V_1=-0.67$ eV obtained numerically from Eq. (4).

Alternatively, by tuning the mass ratio m_1/m_0, in Fig. 3(b), we also demonstrate the existence of p- and d-wave resonant scattering channels. Here, a negative effective mass for the quantum scatterer is used, in order to have resonance conditions in these channels. Applying analytical formula of Eq. (12), the corresponding effective mass for p- and d-wave resonances give $-0.107m_e$ and $-0.1359m_e$, respectively, close to $-0.107m_e$ and $-0.136m_e$ obtained numerically. It is also similar to the plasmonics in electromagnetic waves, where the bandwidth with respect to the parameter variation is much narrow for higher angular momentum resonances. We should remark that without the parameter space illustrated in Fig. 2 and the analytical formulas derived in Eqs. (12)–(13), it is hard to systematically find out the suitable parameters for resonance scattering. On resonances a dramatic change in the direction of momentum in scattering particles is expected, leading to the resonant transport cross section.

In Fig. 4 (a–b), we show the corresponding probability current and probability density for the s-wave at the resonance condition, respectively. At the resonance, the amplitude of scattering coefficient at monopole channel is exactly one; while the contributions from all other channels are significantly reduced. One can find that there exists a reversed current (point to the negative z direction) around the lower hemisphere of scatterer. The maximization of probability density arises nearly at the center of scatterer, but the contribution from higher-order channels leads to an offset.

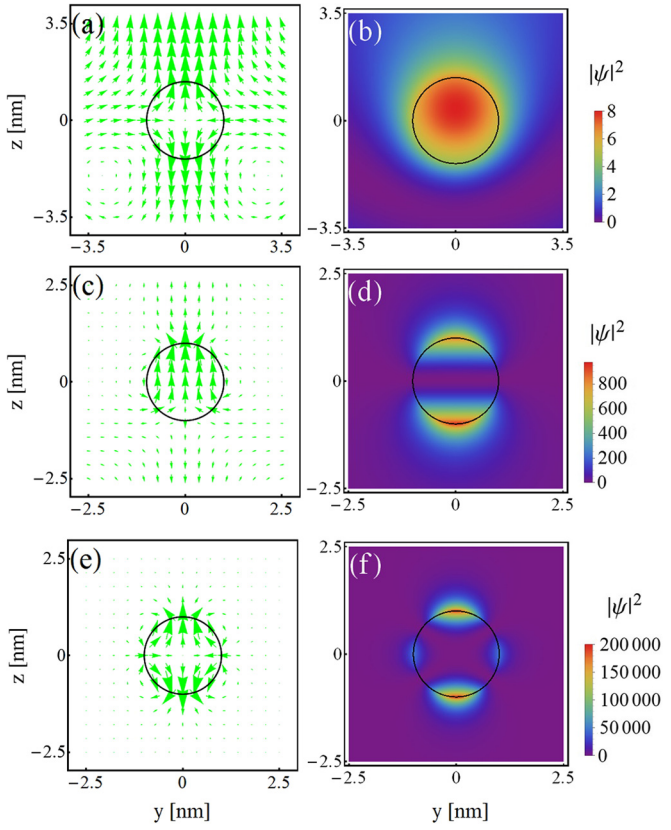

Fig. 4. (Color online.) Probability current and probability density for (a–b): *s*-wave; (c–d): *p*-wave; and (e–f): *d*-wave resonances, respectively. Here, the parameters used are in (a–b) $a = 1.4$ nm, $m_0 = 0.1m_e$, $E = 0.03$ eV, $m_1 = 0.03m_e$ and $V_1 = -0.6$ eV; in (c–d) $a = 1$ nm, $m_0 = 0.2m_e$, $E = 0.02$ eV, $m_1 = -0.11m_e$ and $V_1 = -0.01$ eV; in (e–f) $a = 1$ nm, $m_0 = 0.2m_e$, $E = 0.02$ eV, $m_1 = -0.14m_e$ and $V_1 = -0.01$ eV.

Around the scatterer, a higher probability density is found along the forward direction. For *p*- (dipole) and *d*- (quadrupole) waves at the resonance conditions, Figs. 4 (c–d) and (e–f) show the corresponding probability current and probability density, respectively. A higher probability density appears at a larger angle, which reflects a dramatic change in the momentum of quantum particles. These results are consistent with those obtained from the resonant transport cross section in Figs. 3 (a–b).

In electromagnetics, once the stimulus frequency is operated within the well known negative-epsilon frequency (surface localized electromagnetic mode resonance) for small particles, one can observe a large scattered intensity [3]. Similar to the dielectric constants in electromagnetic waves, the effective mass plays crucial role for resonant conditions. For higher angular momentum resonances, with negative masses, similar phenomena with a larger scattered matter wave are also revealed. As shown in Fig. 4, one can easily see a large probability flux existing at large angles. In the representation of probability flux, a larger transport cross section corresponds to a big change in the direction on incident quantum particles after elastic collisions. It also indicates that for a matter wave with a definite momentum in continuum energy eigenstates, there exist some probabilities to find the particles even at large angles.

Before the conclusion, we briefly discuss possible composited materials to realize quantum resonant scatterers with the effective mass and potential revealed by our approach. Even though most conducting electrons possess a positive effective mass, some semiconductor materials supports a negative effective mass in the Γ-valley for the conducting electrons, such as Sn with an effective mass $-0.058m_0$ in the diamond type, $Zn_\alpha Hg_{1-\alpha}Te$ $(0 \le \alpha \le 0.2)$ and $Cd_\alpha Hg_{1-\alpha}Te$ $(0 \le \alpha \le 0.25)$ [32]. With Eq. (12) and the contour plot shown in Fig. 2, we find that possible candidates to realize quantum resonant scatterers are III–V compound semiconductor materials with lattice-matched heterostructure AlSb and GaSb as our environment and scatterer materials, respectively [32]. With a straddling alignment of energy band-structures, the conducting Γ-valley electron in such a host semiconductor can satisfy the *s*-wave resonance condition, with the effective masses $m_0 = 0.14m_e$ and $m_1 = 0.04m_e$ for AlSb and GaSb, respectively, corresponding to $m_1/m_0 = 0.28$. Suppose the energy for such a conducting electron is $E = 0.03$ eV; then the conduction band offset of GaSb to AlSb is $E_c = -0.5$ eV, corresponding to a well potential, $V_1 = -0.53$ eV. With these parameters, the corresponding size of a quantum resonant scatterer is found to be $a = 1.25$ nm. Moreover, the corresponding size parameters $(k_0 a)^2 = 0.17$ and $(k_1 a)^2 = 0.85$ are both within the subwavelength scale.

4. Conclusion

In summary, by applying the second-order approximation to an isotropic scatterer, beyond the extreme small de Broglie subwavelength approximation, we find the system parameters to satisfy the resonance condition for each angular momentum channels. With the contour plot, all the system parameters, including the geometric radius of a spherical scatterer, the incident energy, effective mass in the environment, effective mass inside the scatterer, and the effective potential inside the scatterer, can be revealed in a single map. Our analytical formulas also provide useful tools to design a resonant quantum system on various angular momentum channels. We find that to excite higher order angular momentum channels, $l \ge 1$, negative mass ratio of $\frac{m_1}{m_0}$ is necessary, which could be used to design a peculiar effective mass-dependent sensor. Moreover, both barrier and well potentials can meet each resonant conditions, which is different from the traditional concept on atomic collision system with attractive potentials. Our analytical formulas and the corresponding contour plot obtained with the second-order expansion provide an accurate approximation for each resonant channels at the subwavelength scale. With the analogy in wave scattering systems, the second-order approach demonstrated in this work may be readily applied to electromagnetic and acoustic systems. Our work promotes potential applications in thermoelectric science, imaging of partial wave interferences, semiconductor defect engineering, quantum sensing, and verification of invisible cloaks.

References

[1] L. Rayleigh, On the light from the sky, its polarization and colour appendix, Philos. Mag. 41 (1871) 107.
[2] C.F. Bohren, D.R. Huffman, Absorption and Scattering of Light by Small Particles, Wiley, New York, 1983.
[3] M.I. Tribelsky, B. Luk'yanchuk, Anomalous light scattering by small particles, Phys. Rev. Lett. 97 (2006) 263902.
[4] M.I. Tribelsky, Anomalous light absorption by small particles, Europhys. Lett. 94 (2011) 14004.
[5] H. Noh, Y.D. Chong, A.D. Stone, H. Cao, Perfect coupling of light to surface plasmons by coherent absorption, Phys. Rev. Lett. 108 (2012) 186805.
[6] K.R. Catchpole, A. Polman, Plasmonic solar cells, Opt. Express 16 (2008) 21793–21800.
[7] J.-Y. Lee, M.-C. Tsai, P.-C. Chen, T.-T. Chen, K.-L. Chan, C.-Y. Lee, R.-K. Lee, Thickness effects on light absorption and scattering for nanoparticles in shape of hollow-spheres, J. Phys. Chem. C 119 (2015) 25754–25760.
[8] L.R. Hirsch, R.J. Stafford, J.A. Bankson, S.R. Sershen, B. Rivera, R.E. Price, J.D. Hazle, N.J. Halas, J.L. West, Nanoshell-mediated near-infrared thermal therapy of tumors under magnetic resonance guidance, Proc. Natl. Acad. Sci. USA 100 (2003) 13549–13554.
[9] M.I. Tribelsky, A.E. Miroshnichenko, Y.S. Kivshar, B.S. Luk'yanchuk, A.R. Khokhlov, Laser pulse heating of spherical metal particles, Phys. Rev. X 1 (2011) 021024.

[10] J.Y. Lee, R.-K. Lee, Phase diagram for passive electromagnetic scatterers, Opt. Express 24 (2016) 6480–6489.
[11] S. Zhang, D.A. Genov, C. Sun, X. Zhang, Cloaking of matter waves, Phys. Rev. Lett. 100 (2008) 123002.
[12] A. Greenleaf, Y. Kurylev, M. Lassas, G. Uhlmann, Approximate quantum cloaking and almost trapped states, Phys. Rev. Lett. 101 (2008) 220404.
[13] D.H. Lin, Cloaking spin-1/2 matter waves, Phys. Rev. A 81 (2010) 063640.
[14] D.H. Lin, Cloaking two-dimensional fermions, Phys. Rev. A 84 (2011) 033624.
[15] D.H. Lin, Transformation design method for quantum states, Phys. Rev. A 85 (2012) 053605.
[16] B.L. Liao, M. Zebarjadi, K. Esfarjani, G. Chen, Cloaking core-shell nanoparticles from conducting electrons in solids, Phys. Rev. Lett. 109 (2012) 126806.
[17] R. Fleury, A. Alú, Quantum cloaking based on scattering cancellation, Phys. Rev. B 87 (2013) 045423.
[18] J.Y. Lee, R.-K. Lee, Hiding the interior region of core-shell nanoparticles with quantum invisible cloaks, Phys. Rev. B 89 (2014) 155425.
[19] M. Zebarjadi, B.L. Liao, K. Esfarjani, M.S. Dresselhaus, G. Chen, Enhancing the thermoelectric power factor by using invisible dopants, Adv. Mater. 25 (2013) 1577–1582.
[20] B.L. Liao, M. Zebarjadi, K. Esfarjani, G. Chen, Isotropic and energy-selective electron cloaks on graphene, Phys. Rev. B 88 (2013) 155432.
[21] W. Shen, T. Tian, B. Liao, M. Zebarjadi, Combinatorial approach to identify electronically cloaked hollow nanoparticles, Phys. Rev. B 90 (2014) 075301.
[22] J.J. Sakurai, J.J. Napolitano, Modern Quantum Mechanics, Pearson Higher Education, 2014.
[23] J.-H. Bahk, P. Santhanam, Z. Bian, R. Ram, A. Shakouri, Resonant carrier scattering by core-shell nanoparticles for thermoelectric power factor enhancement, Appl. Phys. Lett. 100 (2012) 012102.
[24] S.V. Faleev, F. Léonard, Theory of enhancement of thermoelectric properties of materials with nanoinclusions, Phys. Rev. B 77 (2008) 214303.
[25] M. Zebarjadi, K. Esfarjani, A. Shakouri, J.-H. Bahk, Z. Bian, G. Zeng, J. Bowers, H. Lu, J. Zide, A. Gossard, Effect of nanoparticle scattering on thermoelectric power factor, Appl. Phys. Lett. 94 (2009) 202105.
[26] N.R. Thomas, N. Kjærgaard, P.S. Julienne, A.C. Wilson, Imaging of s and d partial-wave interference in quantum scattering of identical bosonic atoms, Phys. Rev. Lett. 93 (2004) 173201.
[27] M.A. Topinka, R.M. Westervelt, E.J. Heller, Imagine electron flow, Phys. Today 56 (2003) 47–52.
[28] E.J. Heller, Quantum proximity resonances, Phys. Rev. Lett. 77 (1996) 4122.
[29] R. Buczko, F. Bassani, Bound and resonant electron states in quantum dots: the optical spectrum, Phys. Rev. B 54 (1996) 2667.
[30] A. Böhm, Quantum Mechanics: Foundations and Applications, 3rd ed., Springer-Verlag, New York, 1993.
[31] R.E. Hamam, A. Karalis, J.D. Joannopoulos, M. Soljacić, Coupled-mode theory for general free-space resonant scattering of waves, Phys. Rev. A 75 (2007) 053801.
[32] S. Adachi, Properties of Group-IV, III–V, and II–VI Semiconductors, John Wiley & Sons Ltd, England, 2005.